UW CPTC Report 10-1 (submitted to Physical Review Letters)
Observation of peak neoclassical toroidal viscous force in the DIII-D tokamak

A. J. Cole,[1] J. D. Callen,[1] W. M. Solomon,[2] A. M. Garofalo,[3] C. C. Hegna,[1] H. Reimerdes,[4] and the DIII-D Team[3]

[1]*University of Wisconsin, Madison, Wisconsin 53706-1609, USA*
[2]*Princeton Plasma Physics Laboratory, P.O. Box 451, Princeton, New Jersey 08543-0451, USA*
[3]*General Atomics, P.O. Box 85608, San Diego, California 92186-5608, USA*
[4]*Columbia University, 2960 Broadway, New York, New York 10027-1754, USA*

(Dated: July 21, 2010)

Observation of a theoretically-predicted peak in the neoclassical toroidal viscosity [NTV] force as a function of toroidal plasma rotation rate Ω is reported. The NTV was generated by applying $n = 3$ magnetic fields from internal (I-)coils to low Ω plasmas produced with nearly balanced neutral beam injection. Locally, the peak corresponds to a toroidal rotation rate Ω_0 where the radial electric field E_r is near zero as determined by radial ion force balance. The value of Ω_0 depends critically on the poloidal rotation value, and is consistent with conventional axisymmetric neoclassical theory.

Understanding the influence of non-axisymmetric (NA) magnetic fields on toroidal plasma rotation remains a fundamental challenge of fusion plasma science. In this paper we investigate the toroidal rotation dependence of neoclassical toroidal viscosity (NTV) driven by NA magnetic perturbations (i.e., those which have some toroidal angular dependence). NA magnetic fields are always present, stemming from either machine errors in coil alignment, current leads, etc., of the order of $\delta B/B_0 \sim 10^{-4}$, or from magnetohydrodynamic [MHD] mode activity, with $\delta B/B_0 \sim 10^{-3}$. Here $B_0 \sim 1-2$ Tesla is the typical equilibrium magnetic field strength for present tokamaks such as DIII-D [1].

One important effect of NA magnetic fields is their modification of $|\vec{B}|$ along a magnetic field-line. Breaking toroidal symmetry introduces bounce-averaged mirror and curvature forces with toroidal components that when crossed with the equilibrium magnetic field generate non-ambipolar radial particle and heat fluxes. In a fluid moment approach [2] toroidal forces arising from symmetry breaking appear as a modification to the parallel stress tensor, generating a *toroidal* viscous force which is absent in the limit of perfect axisymmetry.

When the NA magnetic field amplitude is much less than the poloidal mirror trapping, i.e., $\delta B/B_0 \ll \epsilon = r/R_0$, poloidal and *toroidal* plasma flows on magnetic flux surfaces can be determined successively [3, 4]. First, on the ion-ion collision timescale $1/\nu_i$ ($\sim$ msec), the parallel force balance equation describes the damping of poloidal flow to a diamagnetic-like rate given by $\left\langle q\vec{V}_i \cdot \vec{\nabla}\theta \right\rangle \simeq (c_p/Z_i e) dT_i/d\chi$. (c_p is often labeled k_i [5]). Here $\vec{V}_i$ is the ion fluid velocity, T_i is the ion temperature, $Z_i e$ is the dominant ion species charge, χ is the poloidal magnetic flux function, $q = \vec{B}\cdot\vec{\nabla}\zeta/\vec{B}\cdot\vec{\nabla}\theta = d\Psi/d\chi$ is the toroidal "safety factor," θ (ζ) is a poloidal (toroidal) angle, c_p is a number of order unity, and $\langle \dots \rangle$ denotes a flux surface average. Second, on a longer transport timescale roughly of order $[\nu_i(\delta B_n/B_0)^2]^{-1}$, the NA magnetic fields damp the *toroidal* component of plasma flow to a rotation rate $\Omega_*(\nu_i, E_r) = [(c_t + c_p)/(Z_i e)] dT_i/d\chi$, where c_t is a number of order unity. In this two-stage successive determination of the plasma flows, the NTV damping rate has the form [3, 6, 7]

$$\frac{\partial \Omega}{\partial t} = -\mu_{\|}(\nu_i, E_r) \left\langle \frac{\delta B_n^2}{B_0^2} \right\rangle \left[\Omega - \Omega_*(\nu_i, E_r) \right]. \qquad (1)$$

Here $\left\langle \delta B_n^2/B_0^2 \right\rangle$ is the relative amplitude of the NA fields, $\Omega \equiv \left\langle R^2 \vec{V} \cdot \vec{\nabla}\zeta \right\rangle / \left\langle R^2 \right\rangle$, and $\mu_{\|}(\nu_i, E_r)$ is the NTV damping rate.

Experiments on DIII-D [8], JET [9], NSTX [10], and MAST [11] have all observed toroidal flow damping with the application of external NA fields in general agreement with the form given in (1). With the recent introduction of both co- and counter-I_p neutral beam injection, the DIII-D tokamak is now able to access low toroidal rotation states and observe both toroidal flow damping and spin-up [12, 13], to an offset value in qualitative agreement with Ω_* defined in (5) below.

In this paper, we expand on previous work by performing a rotation scan of the NTV torque applied by external non-resonant $n = 3$ fields from the I-coils [14] on the DIII-D tokamak. Varying the toroidal precessional drift relative to other characteristic frequencies of interest causes a change in the level of NTV damping [15–17]. As will be shown below, scanning toroidal rotation is equivalent to varying the radial electric field, and thus will induce a transition between asymptotic NTV collisionality regimes of interest to tokamaks.

Time scales longer than compressional Alfvén wave times ($\sim \mu$sec) require radial force balance, which yields [3, 4]

$$\omega_E = \frac{\left\langle qR^2\, \vec{V}_i \cdot \vec{\nabla}\theta \right\rangle}{\left\langle R^2 \right\rangle} - \frac{1}{Z_i e n_i} \frac{dp_i}{d\chi} - \Omega \equiv \Omega_0 - \Omega, \qquad (2)$$

where $\omega_E \equiv d\phi/d\chi \simeq E_r/(RB_\theta)$ is the toroidal $\vec{E}\times\vec{B}$ precessional drift frequency.

If the plasma profiles are assumed to remain fixed, then (2) indicates that scanning Ω will cause a concomitant change in E_r. This will in turn vary the critical collisionality ratio ν_i/ω_E, and cause transitions between the relevant NTV regimes.

For DIII-D H-mode plasmas, the relevant NTV regimes are the $1/\nu$ [15], $\sqrt{\nu}$ [16], and the superbanana-plateau [sbp] [17] regimes. We connect the three regimes by Padé approximation:

$$\frac{\partial\Omega}{\partial t} = -\mu_{\|\mathrm{P}}(\Omega)\left\langle\frac{\delta B_n^2}{B_0^2}\right\rangle\left[\Omega-\Omega_*(\Omega)\right], \tag{3}$$

$$\mu_{\|\mathrm{P}}(\Omega) = \frac{0.21|n|v_{ti}^2\sqrt{\epsilon\hat{\nu}}}{\langle R^2\rangle\left[|\omega_E|^{3/2}+0.30|\omega_{\nabla B}|\sqrt{\hat{\nu}}+0.04\hat{\nu}^{3/2}\right]}. \tag{4}$$

The smoothed NTV offset frequency is

$$\Omega_*(\Omega) \equiv \frac{c_p + c_t(\Omega)}{Z_i e}\frac{dT_i}{d\chi}, \tag{5}$$

$$c_t(\Omega) = \frac{2.84\,|\omega_E|^{3/2}+0.84|\omega_{\nabla B}|\sqrt{\hat{\nu}}+0.10\hat{\nu}^{3/2}}{|\omega_E|^{3/2}+0.34|\omega_{\nabla B}|\sqrt{\hat{\nu}}+0.02\hat{\nu}^{3/2}} - \frac{5}{2}. \tag{6}$$

Here $|\omega_E|$ should be expanded via (2), $\hat{\nu}\equiv\nu_i/(|n|\epsilon)$ for compactness, and n is the toroidal mode number of the applied NA field. The grad-B drift frequency for superbananas is $\omega_{\nabla B}$, estimated for thermal particles as $|\omega_{\nabla B}| \equiv T_j/(|Z_j e|)\,|d\epsilon/d\chi|$ [17], and $v_{ti}\equiv\sqrt{2T_i/m_i}$ is the ion thermal speed. For simplicity, we have taken only the very deep sbp regime, in the limit $E_r\to 0$, and thus eliminated any pitch-angle dependence on the toroidal precessional drift or the need for pitch-angle integrals. A more complete connection formula between asymptotic regimes will be left to a future publication. The emphasis here is on the existence of an experimental peak in the NTV torque at low E_r (i.e., $|\omega_E|\to 0$), which is predicted by (3).

The Padé approximant damping rate $\mu_{\|\mathrm{p}}(\Omega)$ is a strongly peaked function of Ω around Ω_0, where $E_r\simeq 0$. Near this peak, (4) reduces to either the sbp regime for $\nu_i/(|n|\epsilon) < 7.5\,|\omega_{\nabla B}|$ or the $1/\nu$ regime when the converse is true. Outside of the peaked region, (4) quickly transitions to the $\sqrt{\nu}$ regime.

Integrating the flux-surface-averaged NTV damping rate over the plasma volume via $\int dV\,[\mathrm{Eq.}\,(3)]\,\langle R^2\rangle\,\rho_M$ yields the total NTV torque on the plasma. In the large aspect-ratio limit this reduces to

$$-T_{NTV} = 4\pi^2 R_0^3\int_0^a r dr\rho_M\mu_{\|\mathrm{P}}^{\mathrm{cyl}}\left\langle\frac{\delta B_n^2}{B_0^2}\right\rangle(\Omega-\Omega_*)^{\mathrm{cyl}}. \tag{7}$$

Here the superscript "cyl" denotes we have approximated $\Omega\equiv\left\langle R^2\vec{V}\cdot\vec{\nabla}\zeta\right\rangle/\langle R^2\rangle\sim V_\phi/R$ along the outboard midplane in what follows.

To investigate the existence of the peak in the total NTV torque predicted by the combination of (4) and (7), NA magnetic field perturbations are applied to DIII-D plasmas using the I-coils: a set of 12 picture-frame coils toroidally distributed at two poloidal locations, six above and six below the midplane [14]. For this experiment, the I-coils are configured in "odd-parity" (the upper set of coils are out of phase with the lower set by 180°) to apply predominantly non-resonant $n=3$ magnetic fields. The DIII-D plasmas presented in this paper are high $\beta_N\sim 1.6-1.7$, high confinement (H-mode) discharges, and have similar lower single null diverted cross sections. Typical ion density, ion temperature, and toroidal rotation profiles along the outboard midplane using NCLASS [18] are shown in Fig. 1.

The total NTV torque dependence on toroidal rotation is observed by making several plasmas with similar safety factor q, density, and temperature, but different toroidal rotation Ω. In each shot, the density, temperature, β_N, and toroidal rotation Ω (determined by a preprogrammed neutral beam injected [NBI] torque) are allowed to reach steady-state (see Fig. 2). To measure the dependence of the radially integrated total NTV torque (7) on toroidal rotation the neutral beams are operated in rotation feedback mode, attempting to hold the observed CER carbon impurity rotation, Ω_C, at the $\rho=0.67$ surface constant. While the beams are on rotation feedback, the I-coils are rapidly switched on at $t\simeq 2050$ ms to 3 kA. As is clear in Fig. 2, the neutral beams maintain the $\rho=0.67$ impurity rotation value of $\Omega_C\simeq 10$ krad/s; but this requires $\Delta T_{NBI}\sim 1$ Nm *less* counter-I_p injected neutral beam torque after the I-coil $n=3$ fields are applied. As shown in Fig. 1, the beam feedback successfully keeps the equilibrium profiles fixed at $\rho=0.67$ (vertical dashed line).

The total NTV torque applied by the I-coils, i.e., that given by (7), can be read directly from the jump in the beam torque: $\Delta T_{NBI}=-T_{NTV}(\Omega)$ as seen in Fig. 2 and is calculated using TRANSP [19]. For this particular shot, 138574, the toroidal rotation rate at the $\rho=0.67$ surface is $\Omega_C\simeq 10$ krad/s. This torque measurement procedure is repeated for several similar discharges, with different Ω_C values on the $\rho=0.67$ surface. The resultant total NTV torque as a function of the deuterium toroidal rotation rate, Ω_D, (calculated from Ω_C using NCLASS) at the $\rho=0.67$ surface is shown by the diamonds plotted in Fig. 3.

To compare the NTV torque predicted by (7) with the experimental data, NCLASS profiles along the outboard midplane are calculated for each shot. The non-resonant magnetic perturbation profile $\langle\delta B_n^2(r)/B_0^2\rangle$ from the applied $n=3$ fields is assumed to be a *vacuum* cylindrical profile $\langle\delta B_n^2(r)/B_0^2\rangle = |b_{m3,\theta}(a)|^2/B_0^2(r/a)^{2m-2}$ for a single $m,n=3$ perturbation. However, the absolute value of the poloidal component of the magnetic perturbation at the plasma edge $|b_{m3,\theta}(a)|$ is estimated by calculating the volume-averaged squared magnetic pertur-

bation strength $\left\langle \delta B_n^2(r) \right\rangle_{\rm vol} = |b_{m3,\theta}(a)|^2/m$ and setting that equal to $\left\langle \delta B_n^2(r) \right\rangle_{\rm vol}$ obtained by MARS-F simulations for similar DIII-D discharges with an applied $n = 3$ field (see Fig. 10 in [13]). For simplicity, we assume a single $m = 2, n = 3$ magnetic perturbation, which would give $|b_{23,\theta}(a)| \simeq 4.7 \times 10^{-3}$ Tesla using an I-coil current of 3 kA, or $|b_{23,\theta}(a)/B_0| \simeq 2.4 \times 10^{-3}$ for a typical toroidal field on the magnetic axis of $B_0 = 1.94$ Tesla. The radial electric field profile (2) is calculated in the cylindrical limit via

$$\omega_E^{\rm cyl} \simeq \frac{c_p - 1}{Z_i e} \frac{dT_i}{d\chi} - \frac{T_i}{Z_i e n_i} \frac{dn_i}{d\chi} - \Omega^{\rm cyl}. \qquad (8)$$

A theoretical NTV torque scan is performed with (7) using the NCLASS equilibrium for shot 138574 at 2400 ms. The profiles are held fixed, while the deuterium toroidal rotation profile is scanned self-similarly, i.e., $\Omega(\rho) = \Omega f(\rho)$, where $-30 \le \Omega \le 15$ krad/sec and $f(\rho) \equiv \Omega(\rho)/\Omega(0.67)$ is a normalized rotation profile from shot 138574 at 2400 ms. The computed torque as a function of Ω is shown by the solid line labeled "model" in Fig. 3. In addition, the NTV torque (7) is calculated for each NCLASS plasma equilibrium independently and plotted (triangles) in the same figure. In all cases, the profiles are integrated from $\rho = 0.1$ to 0.9. The point NTV rotation scan (triangles) is calculated by taking the average of the computed torque profile ~ 100 ms before and ~ 400 ms after the I-coil switch-on.

Good agreement between the model (line), the theory points (triangles), and the data (diamonds) for the location of the peak in Fig. 3 is obtained by fitting the unknown value of the equilibrium neoclassical poloidal rotation constant c_p to a value of $c_p = 1.4$. The width of the peak predicted by theory is narrower than the data by a factor of 3. From a theoretical viewpoint, this is not surprising since we have used a Padé approximation between asymptotic regimes which does not smooth over pitch angle and particle energy.

Using NCLASS, we may estimate c_p using

$$c_p^{\rm NCLASS} \equiv c_p^N \simeq Z_i e\, U_{\theta,i}\, B_0^2 \left(B_t R\, dT_i/d\chi\right)^{-1}, \qquad (9)$$

where $U_{\theta,i} \equiv \vec{V}_i \cdot \vec{\nabla}\theta / (\vec{B} \cdot \vec{\nabla}\theta)$, and B_t is the toroidal component of the magnetic field. For shot 138574 at 2400 ms, Eq. (9) varies from $c_p^N = 0.9$ at $\rho = 0.1$ to $c_p^N = 0.7$ at $\rho = 0.7$, and falls sharply to $c_p^N = 0.3$ at $\rho = 0.9$. To estimate the error in determining c_p from our model, (7) is plotted against the data for three different choices of the poloidal rotation coefficient c_p in the top plot of Fig. 4. The torque curve for the best fit value of $c_p = 1.4$ is well bracketed by the two curves with $c_p = 1.4 \pm 0.6$, respectively. Thus the c_p^N values for $\rho < 0.7$ are close to our error bars, but the c_p^N values falling below 0.8 as ρ increases from 0.7 would place the NTV theory model peak beyond (in the co-I_p direction) the experimental data in the top panel of Fig. 4.

The center panel in Fig. 4 shows a representative NTV torque density profile for $c_p = 1.4$. Local maxima exist everywhere the radial electric field vanishes as determined by (8) and shown with ω_E in the lower panel in Fig. 4. Inspecting the lower panel of Fig. 1, the largest torque peak in the radial profile shown occurs when the $1/\nu$ and sbp regimes *both* contribute to the NTV. However, this is partly a consequence of our $\left\langle \delta B_n^2(r)/B_0^2 \right\rangle$ profile which is largest at the plasma edge.

In summary, this paper reports the first observation of a theoretically-predicted peak in the NTV torque for low toroidal rotation rates, $-10 < \Omega < 5$ krad/s, in DIII-D by applying external $n = 3$ NA magnetic fields with the I-coils. The experimental peak is found to be in good agreement with a simple Padé approximant connection formula calculated in the large aspect-ratio, cylindrical tokamak limit. These results are significant in demonstrating that the $\vec{E} \times \vec{B}$ and diamagnetic-level poloidal and toroidal flows and the torques on them discussed here and in [12, 13] are as predicted by a combination of axisymmetric and NA neoclassical theory. NTV has the potential to alter rotation profiles in low external torque configurations for a variety of applications in ITER.

This research was supported by the U.S. Department of Energy under Grant Nos. DE-FG02-86ER53218, DE-FG02-92ER54139, DE-FG02-99ER54546, DE-FC02-04ER54968, DE-FG02-89ER53297 and DE-AC02-09CH11466. Figures were generated using Scilab ®: `http://www.scilab.org`.

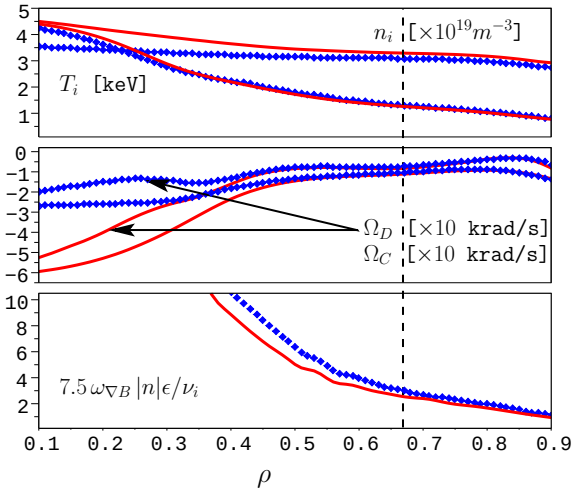

FIG. 1: (top, center) NCLASS plasma profiles for shot 138574 at $t = 1900$ ms (solid line) and $t = 2400$ ms (marker). Vertical dashed line shows surface where CER feedback was performed. (lower) Plot indicating $\nu_i/(|n|\epsilon) < 7.5|\omega_{\nabla B}|$ over most of the plasma profile and thus the peak NTV torque is governed by the sbp regime [17] until $\rho \ge 0.8$ where the sbp and $1/\nu$ [15] regimes become comparable in this model.

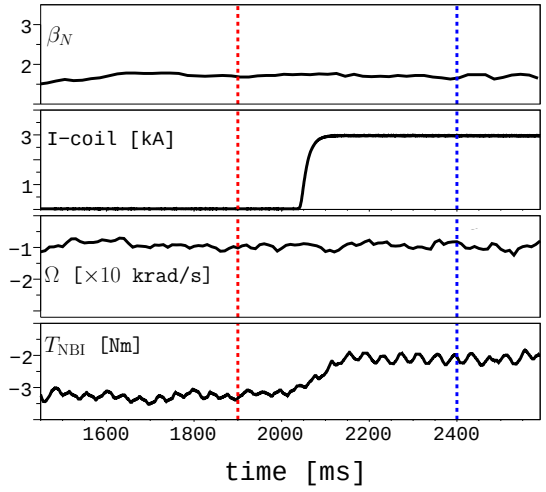

FIG. 2: Experimental time trace for shot 138574, showing β_N, I-coil current, rotation rate at $\rho = 0.67$, and the total injected neutral beam torque. Positive rotation and NBI torque are both in the co-Ip direction. Vertical dashed lines refer to the profiles plotted in Fig. 1 before ($t = 1900$ ms) and after ($t = 2400$ ms) I-coil switch-on.

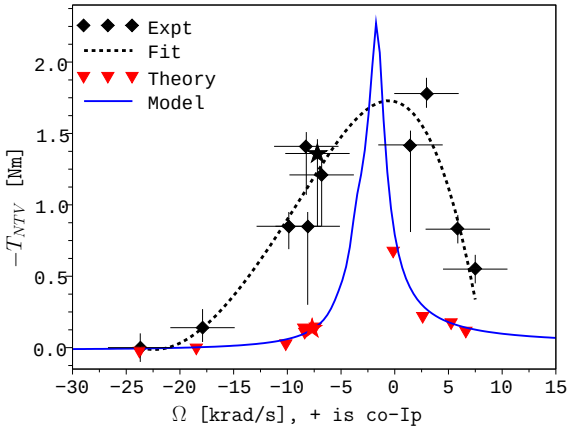

FIG. 3: Comparison of measured NTV (diamonds), and cylindrical torque model (line) versus deuterium toroidal rotation rate (obtained from NCLASS) at $\rho = 0.67$. A least-squares spline fit (dashed) is shown for the data. Individual NTV torque points (triangles) are shown for each shot by taking the average of (7) computed slightly before and after I-coil switch-on. The starred points indicate shot 138574.

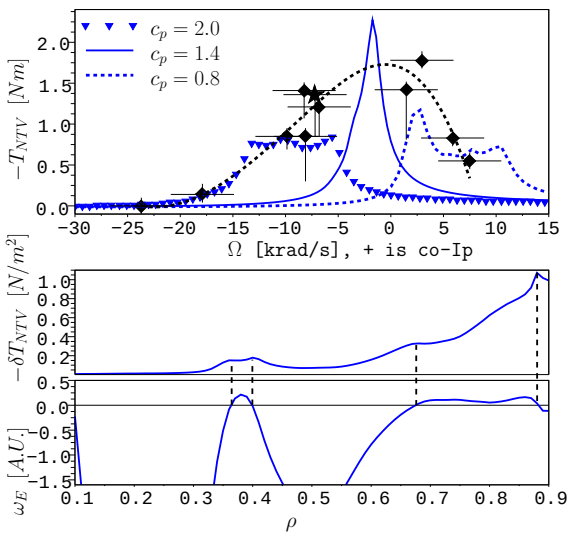

FIG. 4: (top) Total cylindrical $(m, n = 2, 3)$ NTV torque integrated over the plasma profile as a function of Ω at $\rho = 0.67$; symbols are as in Fig. 3. Varying only the poloidal rotation value, c_p, the best fit is $c_p = 1.4$ (solid line) bracketed by two other curves with $c_p = 1.4 \pm 0.6$ respectively. Representative torque density (center) for $c_p = 1.4$, which has local maxima where $\omega_E \simeq 0$ (lower plot) and indicated with vertical dashed lines.

[1] J. L. Luxon, M. J. Schaffer, G. L. Jackson, et al., Nucl. Fus. **43**, 1813 (2003).

[2] K. C. Shaing and J. D. Callen, Phys. Fluids **26**, 3315 (1983).

[3] J. D. Callen, A. J. Cole, and C. C. Hegna, Nucl. Fus. **49**, 085021 (2009).

[4] J. D. Callen, A. J. Cole, and C. C. Hegna, Phys. Plasmas **16**, 082504 (2009).

[5] F. L. Hinton and R. D. Hazeltine, Rev. Mod. Phys. **48**, 239 (1976).

[6] A. J. Cole, C. C. Hegna, and J. D. Callen, Phys. Rev. Lett. **99**, 065001 (2007).

[7] A. J. Cole, C. C. Hegna, and J. D. Callen, Phys. Plasmas **15**, 056102 (2008).

[8] R. J. La Haye, S. Günter, D. A. Humphreys, et al., Phys. Plasmas **9**, 2051 (2002), see p. 2058.

[9] E. Lazzaro, R. J. Buttery, T. C. Hender, et al., Phys. Plasmas **9**, 3906 (2002).

[10] W. Zhu, S. A. Sabbagh, R. E. Bell, et al., Phys. Rev. Lett. **96**, 225002 (2006).

[11] M.-D. Hua, I. T. Chapman, A. R. Field, et al., Plasma Phys. and Control. Fusion **52**, 035009 (2010).

[12] A. M. Garofalo, K. H. Burrell, J. C. DeBoo, et al., Phys. Rev. Lett. **101**, 195005 (2008).

[13] A. M. Garofalo, W. M. Solomon, M. Lanctot, et al., Phys. Plasmas **16**, 056119 (2009).

[14] G. L. Jackson, P. M. Anderson, J. Bialek, et al., in *Proceedings 30th EPS Conf. on Contr. Fus. Plas. Physics, St. Petersburg, Russia*, edited by R. Koch and S. Lebedev (2003), Europhysics Conference Abstracts, contributed papers,Vol. 27A, p. P-4.47 CD-ROM.

[15] K. C. Shaing, Phys. Plasmas **10**, 1443 (2003).

[16] K. C. Shaing, P. Cahyna, M. Becoulet, et al., Phys. Plasmas **15**, 082506 (2008).

[17] K. C. Shaing, S. A. Sabbagh, and M. S. Chu, Plasma Phys. and Control. Fusion **51**, 035009 (2009).

[18] W. A. Houlberg, K. C. Shaing, S. P. Hirshman, et al., Phys. Plasmas **4**, 3230 (1997).

[19] R. Hawryluk, in *Phys. of Plas. Close to Thermo. Cond.*, edited by B. Coppi et al. (CEC, Brussels, 1980), p. 19.